Dynamic analysis of the agglomerated SiO₂ nanoparticles-reinforced by concrete blocks with close angled discontinues subjected to blast load

Hassan Bakhshandeh Amnieh[*1] and Mohammad Saber Zamzam[2]

[1]*School of Mining, College of Engineering, University of Tehran, Iran*
[2]*Department of Mining Engineering, Faculty of Engineering, University of Kashan, Iran*

Abstract. Three structure-dependent integration methods with no numerical dissipation have been successfully developed for time integration. Although these three integration methods generally have the same numerical properties, such as unconditional stability, second-order accuracy, explicit formulation, no overshoot and no numerical damping, there still exist some different numerical properties. It is found that TLM can only have unconditional stability for linear elastic and stiffness softening systems for zero viscous damping while for nonzero viscous damping it only has unconditional stability for linear elastic systems. Whereas, both CEM and CRM can have unconditional stability for linear elastic and stiffness softening systems for both zero and nonzero viscous damping. However, the most significantly different property among the three integration methods is a weak instability. In fact, both CRM and TLM have a weak instability, which will lead to an adverse overshoot or even a numerical instability in the high frequency responses to nonzero initial conditions. Whereas, CEM possesses no such an adverse weak instability. As a result, the performance of CEM is much better than for CRM and TLM. Notice that a weak instability property of CRM and TLM might severely limit its practical applications.

Keywords: weak instability; numerical instability; overshoot; structure-dependent integration method

1. Introduction

Blast test in real scale in concrete structure is an important issue for the researchers and industries. But in real scale, there are many problems such as environment, building of sample, combine parameters and etc. Due to the high cost and time consuming of experimental tests, matching a mathematical model for theoretical analysis of the concrete structures subjected to blast is very important which the researchers should study about his field. Our purpose in this article is opening a new field in the mining engineering for theoretical analysis of the concrete blocks under blast.

Blast analysis of different structures has been reported by many researchers. Wu *et al*. (1998) investigated the propagation characteristics of blast-induced shock waves in a jointed rock mass. A systematic and efficient blast analysis procedure for Fiber Reinforced Polymer (FRP) retrofitting design of concrete arch structure was suggested by Nam *et al*. (2009). The procedure was composed of three sequential parts of preliminary analysis, breach and debris analysis, and retrofit-material analysis. Li *et al*. (2009) developed a better understanding of the behavior of steel-concrete composite beams (SCCB) under localized blast loading through a numerical parametric study. A finite element model was set up to simulate the blast-resistant features of SCCB using the transient dynamic analysis

software LS-DYNA. Bayraktar *et al*. (2010) evaluated blast effects on a reinforced concrete (RC) building considering experimentally determined dynamic characteristics. The study consists of three phases: the measurement of vibration characteristics of blasting, the theoretical modal analysis of the inspected building, and experimental verification of dynamic characteristics using modal testing. Li and Ma (2010) carried out quantitative analysis for the interaction between obliquely incident *P*- or *S*-blast wave and a linear elastic rock joint. Petel *et al*. (2011) investigated the interaction of a blast wave with a multilayered material for the purpose of blast wave attenuation. Jayasooriya *et al*. (2011) studied the impact of near field explosions on the reinforced concrete framed buildings and key elements such as columns and describes the component material response.

Debonding failure analysis technique for FRP retrofitted concrete structure under blast loading was suggested by Kim *et al*. (2011) considering FRP material characteristics and debonding failure mechanisms as well as rate dependent failure mechanism based on a blast resisting design concept. Aliabadian *et al*. (2014) used two-dimensional (2D) distinct element method for the dynamic fracture mechanism of blast-induced fracturing of rock mass around a blast hoe. The characteristics of rock fragmentation subjected to blast load by using the hydrocode in the platform of AUTODYN were investigated by Jeon *et al*. (2015). Oña *et al*. (2016) described an experimental campaign carried out to study and analyse the behaviour of concrete slabs when subjected to blast loading. Four different types of concrete have been tested: normal strength concrete with steel rebar, normal strength concrete with steel rebar retrofitted with Kevlar coating, steel fibre

---

*Corresponding author, Ph.D.
 E-mail: hbakhshandeh@ut.ac.ir
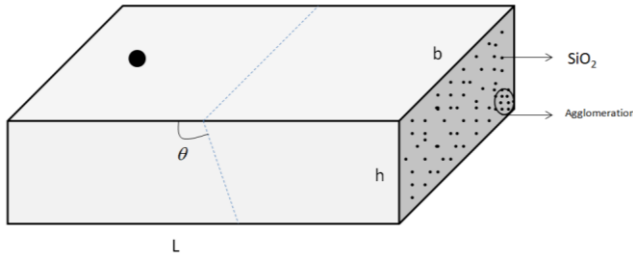
Fig. 1 A schematic view of the concrete block with close angled discontinues

reinforced concrete (SFRC) and polypropylene fibre reinforced concrete (PFRC). Li *et al.* (2016) monitored and analyzed the blasting waves at different blast center distances by the Hilbert-Huang transform (HHT) in a coal mine. Experimental results regarding blast performance of High Strength Fiber Reinforced Concrete (HSFRC) structural elements were presented by Luccioni *et al.* (2017). A numerical study was undertaken by Kyei and Braimah (2017) to investigate the effects of transverse reinforcement spacing on the blast resistance of RC columns. The study shows that the effect of transverse reinforcement spacing and axial loading significantly affects RC column behaviour under blast loading at low scaled distances. Dadsetan and Bai (2017) investigate the mechanical and microstructural properties of self-compacting concrete (SCC) mixtures containing three supplementary cementitious materials (SCMs), namely metakaolin, ground granulated blast-furnace slag and fly ash. Yoo and Banthia (2017) comprehensively investigates impact and blast resistances of ultra-high-performance fiber-reinforced concrete (UHPFRC) by considering various influential factors.

To the best of the author knowledge, no research has been found in the literature for mathematical modeling of concrete blocks under blast load considering the effects of nanotechnology. However, in this paper, for the first time, a mathematical model is presented for blast analysis of concrete blocks reinforced with SiO$_2$ nanoparticles considering agglomeration effects. The governing equation is derived using CPT, energy method and Hamilton's principle. The velocity response of the structure is calculated by exact solution and Newmark method. In addition, the theoretical results are validated with experimental test. The effect of different parameters such as SiO$_2$ nanoparticles volume percent and agglomeration, angle of discontinues, length, width and thickness of the model are shown on the maximum velocity response of the structure.

2. Mathematical modeling

Consider a concrete blocks with close angled discontinues reinforced with agglomerated SiO$_2$ nanoparticles as depicted in Fig. 1 in which geometrical parameters of length *L*, width *b* and thickness *h* are indicated. The Cartesian coordinate is considered in the middle surface of plate in which *x*, *y* and *z* represent the

axial, vertical and transverse directions, respectively. A blast hole before the discontinues is considered with the diameter *D* and height *H*.

2.1 Kinematic of theory

Based on the Mindlin-Reissner theory for thick plates theory, the displacement field for a plate element can be written as (Brush and Almorth 1975)

$$u_1(x,y,z,t) = u(x,y,t) + z\,\phi_x(x,y,t), \qquad (1)$$

$$u_2(x,y,z,t) = v(x,y,t) + z\,\phi_y(x,y,t), \qquad (2)$$

$$u_3(x,y,z,t) = w(x,y,t), \qquad (3)$$

where *u*, *v* and *w* are the mid plane displacement in *x*-, *y*- and *z*- directions, respectively; ϕ_x and ϕ_x are the rotations of cross section about *y*- and *x*- axis, respectively. The strain-displacement relations can be expressed as follows

$$\varepsilon_{xx} = \frac{\partial u}{\partial x} + z\,\frac{\partial \phi_x}{\partial x}, \qquad (4)$$

$$\varepsilon_{yy} = \frac{\partial v}{\partial y} + z\,\frac{\partial \phi_y}{\partial y}, \qquad (5)$$

$$\gamma_{xy} = \frac{\partial v}{\partial x} + \frac{\partial u}{\partial y} + z\left(\frac{\partial \phi_x}{\partial y} + \frac{\partial \phi_y}{\partial x}\right). \qquad (6)$$

$$\gamma_{xz} = \frac{\partial w}{\partial x} + \phi_x, \qquad (7)$$

$$\gamma_{yz} = \frac{\partial w}{\partial y} + \phi_y, \qquad (8)$$

2.2 Mori-Tanaka model

In this section, the effective modulus of the concrete plate reinforced by SiO$_2$ nanoparticles is developed. Different methods are available to obtain the average properties of a composite. Due to its simplicity and accuracy even at high volume fractions of the inclusions, the Mori-Tanaka method (Mori and Tanaka 1973) is employed in this section. The matrix is assumed to be isotropic and elastic, with the Young's modulus E_m and the Poisson's ratio v_m. The constitutive relations for a layer of the composite with the principal axes parallel to the *r*, *θ* and *z* directions are (Mori and Tanaka 1973)

$$\begin{Bmatrix} \sigma_{xx} \\ \sigma_{\theta\theta} \\ \sigma_{zz} \\ \tau_{\theta z} \\ \tau_{xz} \\ \tau_{x\theta} \end{Bmatrix} = \begin{bmatrix} k+m & l & k-m & 0 & 0 & 0 \\ l & n & l & 0 & 0 & 0 \\ k-m & l & k+m & 0 & 0 & 0 \\ 0 & 0 & 0 & p & 0 & 0 \\ 0 & 0 & 0 & 0 & m & 0 \\ 0 & 0 & 0 & 0 & 0 & p \end{bmatrix} \begin{Bmatrix} \varepsilon_{xx} \\ \varepsilon_{\theta\theta} \\ \varepsilon_{zz} \\ \gamma_{\theta z} \\ \gamma_{xz} \\ \gamma_{x\theta} \end{Bmatrix}, \qquad (9)$$

where σ_{ij}, ε_{ij}, γ_{ij}, *k*, *m*, *n*, *l*, *p* are the stress components, the strain components and the stiffness coefficients

respectively. According to the Mori-Tanaka method the stiffness coefficients are given by

$$k = \frac{E_m\{E_m c_m + 2k_r(1+v_m)[1+c_r(1-2v_m)]\}}{2(1+v_m)[E_m(1+c_r-2v_m)+2c_m k_r(1-v_m-2v_m^2)]}$$

$$l = \frac{E_m\{c_m v_m[E_m + 2k_r(1+v_m)]+2c_r l_r(1-v_m^2)]\}}{(1+v_m)[E_m(1+c_r-2v_m)+2c_m k_r(1-v_m-2v_m^2)]}$$

$$n = \frac{E_m^2 c_m(1+c_r-c_m v_m)+2c_m c_r(k_r n_r - l_r^2)(1+v_m)^2(1-2v_m)}{(1+v_m)[E_m(1+c_r-2v_m)+2c_m k_r(1-v_m-2v_m^2)]}$$

$$+ \frac{E_m[2c_m^2 k_r(1-v_m)+c_r n_r(1+c_r-2v_m)-4c_m l_r v_m]}{E_m(1+c_r-2v_m)+2c_m k_r(1-v_m-2v_m^2)} \quad (10)$$

$$p = \frac{E_m[E_m c_m + 2p_r(1+v_m)(1+c_r)]}{2(1+v_m)[E_m(1+c_r)+2c_m p_r(1+v_m)]}$$

$$m = \frac{E_m[E_m c_m + 2m_r(1+v_m)(3+c_r-4v_m)]}{2(1+v_m)\{E_m[c_m + 4c_r(1-v_m)]+2c_m m_r(3-v_m-4v_m^2)\}}$$

where the subscripts m and r stand for matrix and reinforcement respectively. C_m and C_r are the volume fractions of the matrix and the nanoparticles respectively and k_r, l_r, n_r, p_r, m_r are the Hills elastic modulus for the nanoparticles (Mori and Tanaka 1973). The experimental results show that the assumption of uniform dispersion for nanoparticles in the matrix is not correct and the most of nanoparticles are bent and centralized in one area of the matrix. These regions with concentrated nanoparticles are assumed to have spherical shapes, and are considered as ''inclusions'' with different elastic properties from the surrounding material. The total volume V_r of nanoparticles can be divided into the following two parts (Shi and Feng 2004)

$$V_r = V_r^{inclusion} + V_r^m \quad (11)$$

where $V_r^{inclusion}$ and V_r^m are the volumes of nanoparticles dispersed in the spherical inclusions and in the matrix, respectively. Introduce two parameters ξ and ζ describe the agglomeration of nanoparticles

$$\xi = \frac{V_{inclusion}}{V}, \quad (12)$$

$$\zeta = \frac{V_r^{inclusion}}{V_r}. \quad (13)$$

However, the average volume fraction c_r of nanoparticles in the composite is

$$C_r = \frac{V_r}{V}. \quad (14)$$

Assume that all the orientations of the nanoparticles are completely random. Hence, the effective bulk modulus (K) and effective shear modulus (G) may be written as

$$K = K_{out}\left[1 + \frac{\xi\left(\frac{K_{in}}{K_{out}}-1\right)}{1+\alpha(1-\xi)\left(\frac{K_{in}}{K_{out}}-1\right)}\right], \quad (15)$$

$$G = G_{out}\left[1 + \frac{\xi\left(\frac{G_{in}}{G_{out}}-1\right)}{1+\beta(1-\xi)\left(\frac{G_{in}}{G_{out}}-1\right)}\right], \quad (16)$$

where

$$K_{in} = K_m + \frac{(\delta_r - 3K_m\chi_r)C_r\zeta}{3(\xi - C_r\zeta + C_r\zeta\chi_r)}, \quad (17)$$

$$K_{out} = K_m + \frac{C_r(\delta_r - 3K_m\chi_r)(1-\zeta)}{3[1-\xi-C_r(1-\zeta)+C_r\chi_r(1-\zeta)]}, \quad (18)$$

$$G_{in} = G_m + \frac{(\eta_r - 3G_m\beta_r)C_r\zeta}{2(\xi - C_r\zeta + C_r\zeta\beta_r)}, \quad (19)$$

$$G_{out} = G_m + \frac{C_r(\eta_r - 3G_m\beta_r)(1-\zeta)}{2[1-\xi-C_r(1-\zeta)+C_r\beta_r(1-\zeta)]}, \quad (20)$$

where $\chi_r, \beta_r, \delta_r, \eta_r$, may be calculated as

$$\chi_r = \frac{3(K_m+G_m)+k_r-l_r}{3(k_r+G_m)}, \quad (21)$$

$$\beta_r = \frac{1}{5}\left\{\begin{array}{l}\frac{4G_m+2k_r+l_r}{3(k_r+G_m)}+\frac{4G_m}{(p_r+G_m)} \\ +\frac{2[G_m(3K_m+G_m)+G_m(3K_m+7G_m)]}{G_m(3K_m+G_m)+m_r(3K_m+7G_m)}\end{array}\right\}, \quad (22)$$

$$\delta_r = \frac{1}{3}\left[n_r + 2l_r + \frac{(2k_r-l_r)(3K_m+2G_m-l_r)}{k_r+G_m}\right], \quad (23)$$

$$\eta_r = \frac{1}{5}\left[\begin{array}{l}\frac{2}{3}(n_r-l_r)+\frac{4G_m p_r}{(p_r+G_m)}+\frac{2(k_r-l_r)(2G_m+l_r)}{3(k_r+G_m)} \\ +\frac{8G_m m_r(3K_m+4G_m)}{3K_m(m_r+G_m)+G_m(7m_r+G_m)}\end{array}\right]. \quad (24)$$

where, K_m and G_m are the bulk and shear moduli of the matrix which can be written as

$$K_m = \frac{E_m}{3(1-2v_m)}, \quad (25)$$

$$G_m = \frac{E_m}{2(1+v_m)}. \quad (26)$$

Furthermore, β, α can be obtained from

$$\alpha = \frac{(1+v_{out})}{3(1-v_{out})}, \quad (27)$$

$$\beta = \frac{2(4-5v_{out})}{15(1-v_{out})}, \quad (28)$$

$$v_{out} = \frac{3K_{out}-2G_{out}}{6K_{out}+2G_{out}}. \quad (29)$$

Finally, the elastic modulus (E) and poison's ratio (v) can be calculated as

$$E = \frac{9KG}{3K+G}, \quad (30)$$

$$v = \frac{3K-2G}{6K+2G}. \quad (31)$$

2.3 Governing equations

In this section, the energy method and Hamilton's principle are used for deriving the governing equations for the concrete plate reinforced by SiO$_2$ nanoparticles subjected to impact load. The potential energy of the structure can be written as

$$U = \frac{1}{2}\int \left(\sigma_{xx}\varepsilon_{xx} + \sigma_{yy}\varepsilon_{yy} + \tau_{xy}\gamma_{xy} + \tau_{xz}\gamma_{xz} + \tau_{yz}\gamma_{yz} \right)dV, \quad (32)$$

Substituting Eqs. (4) to (8) into Eq. (32) yields the potential energy as follows

$$
U = 0.5 \int_A \left(N_{xx}\frac{\partial u}{\partial x} + N_{yy}\frac{\partial v}{\partial y} + N_{xy}\left(\frac{\partial v}{\partial x} + \frac{\partial u}{\partial y}\right) \right.
$$
$$
+ M_{xx}\frac{\partial \phi_x}{\partial x} + M_{yy}\frac{\partial \phi_y}{\partial x} + 2M_{xy}\left(\frac{\partial \phi_x}{\partial y} + \frac{\partial \phi_y}{\partial x}\right) \quad (33)
$$
$$
\left. + Q_x\left(\frac{\partial w}{\partial x} + \phi_x\right) + Q_y\left(\frac{\partial w}{\partial y} + \phi_y\right) \right)dA,
$$

where the resultant force and moments may be calculated as

$$
\begin{bmatrix} N_{xx} \\ N_{yy} \\ N_{xy} \end{bmatrix} = \int_{-h/2}^{h/2} \begin{bmatrix} \sigma_{xx} \\ \sigma_{yy} \\ \tau_{xy} \end{bmatrix} dz, \quad (34)
$$

$$
\begin{bmatrix} M_{xx} \\ M_{yy} \\ M_{xy} \end{bmatrix} = \int_{-h/2}^{h/2} \begin{bmatrix} \sigma_{xx} \\ \sigma_{yy} \\ \tau_{xy} \end{bmatrix} z\,dz, \quad (35)
$$

$$
\begin{bmatrix} Q_x \\ Q_y \end{bmatrix} = k' \int_{-h/2}^{h/2} \begin{bmatrix} \tau_{xz} \\ \tau_{yz} \end{bmatrix} z\,dz, \quad (36)
$$

where k' is shear correction factor. The kinetic energy of the structure is

$$K = \frac{\rho}{2}\int \left((\dot{u}_1)^2 + (\dot{u}_2)^2 + (\dot{u}_3)^2 \right)dV, \quad (37)$$

where ρ is the density of the structure. The kinetic energy of SSDT can be obtained by substituting Eqs. (1)-(3) into Eq. (37) as follows

$$
K = 0.5 \int \left[I_0\left(\left(\frac{\partial u}{\partial t}\right)^2 + \left(\frac{\partial v}{\partial t}\right)^2 + \left(\frac{\partial w}{\partial t}\right)^2 \right) \right.
$$
$$
\left. + 2I_1\left(\frac{\partial u}{\partial t}\frac{\partial \phi_x}{\partial t} + \frac{\partial v}{\partial t}\frac{\partial \phi_y}{\partial t} \right) + I_2\left(\left(\frac{\partial \phi_x}{\partial t}\right)^2 + \left(\frac{\partial \phi_\theta}{\partial t}\right)^2 \right) \right]dA, \quad (38)
$$

where the moment of inertia in kinetic energy of three theories can be defined as

$$(I_0, I_1, I_2) = \int_{-h/2}^{h/2} \rho\left(1, z, z^2\right)dz. \quad (39)$$

The force done by the blast load can be expressed as (Hause and Librescu 2007, Kinney and Graham 1985)

$$P_{blast} = P_{S0}\left[1 - \frac{t}{t_0}\right]\exp\left\{\frac{-at}{t_0}\right\}, \quad (40)$$

where the maximum pressure of blast (P_{S0}) and the time of positive phase (t_0) are

$$
\frac{P_{S0}}{P_0} = \frac{808\left[1 + \left(\frac{Z}{4.5}\right)^2\right]}{1 + \left(\frac{Z}{0.048}\right)^2\sqrt{1 + \left(\frac{Z}{1.35}\right)^2}}, \quad (41)
$$

$$
\frac{t_0}{W^{1/3}} = \frac{980\left[1 + \left(\frac{Z}{0.54}\right)^{10}\right]}{\left[1 + \left(\frac{Z}{0.02}\right)^3\right]\left[1 + \left(\frac{Z}{0.74}\right)^6\right]\sqrt{1 + \left(\frac{Z}{6.9}\right)^2}}, \quad (42)
$$

where P_9 is atmosphere pressure and Z is

$$Z = \frac{R}{W^{0.33}}, \quad (43)$$

where R is the distance of center of blast to center are of the structure and W is the mass of explosive materials in terms of TNT.

The force of the angled surface crack to the structure is (Ismail and Cartmell 2012)

$$
n_x\frac{\partial^2 w}{\partial x^2} + \frac{aD(1 + \cos 2\beta)}{3\left(\frac{\alpha_{bt}}{6} + \alpha_{bb}\right)(3 + v)(1 - v)h + 2a}
$$
$$
\left(\frac{\partial^3 \phi_y}{\partial y^3} + v\frac{\partial^3 \phi_x}{\partial x^2 \partial y}\right) - \frac{a(1 + \cos 2\beta)}{(6\alpha_{tb} + \alpha_{tt})(1 - v^2)h + 2a}n_y\frac{\partial^2 w}{\partial y^2}
$$
$$
+ \frac{2a\sin 2\beta}{3\left(\frac{C_{bt}}{6} + C_{bb}\right)(1 + v)h + 2a}\left(\frac{\partial^4 \phi_y}{\partial x \partial y^2} + v\frac{\partial^4 \phi_x}{\partial x^2 \partial y}\right) \quad (44)
$$
$$
- \frac{2a\sin 2\beta}{(6C_{tb} + C_{bttb})(1 + v)h + 2a}n_y\frac{\partial^2 w}{\partial x \partial y},
$$

where $D = Eh^3/12(1 - v^2)$ is the flexural rigidity of the concrete structure with E, v and h representing the modulus of elasticity, plate thickness and Poisson ratio, respectively. The non-dimensional compliance coefficients α_{bt}, α_{bb}, α_{tb}, α_{tt} and C_{bt}, C_{bb}, C_{tb}, C_{tt} are reported by Rice and Levy (1972), Joseph and Erdogan (1991), Lu and Xu (1986).

The motion equations can be derived based on Hamilton's principle as follows

$$\int_0^t (\delta U - \delta W - \delta K)dt = 0. \quad (45)$$

Substituting the energies into Eq. (45) yields the motion equations as

$$\delta u: \quad \frac{\partial N_{xx}}{\partial x} + \frac{\partial N_{xy}}{\partial y} = I_0\frac{\partial^2 u}{\partial t^2} + I_1\frac{\partial^2 \phi_x}{\partial t^2}, \quad (46)$$

$$\delta v: \quad \frac{\partial N_{xy}}{\partial x} + \frac{\partial N_{yy}}{\partial y} + \frac{Q_y}{R} = I_0\frac{\partial^2 v}{\partial t^2} + I_1\frac{\partial^2 \phi_\theta}{\partial t^2}, \quad (47)$$

$$
\delta w: \quad \frac{\partial Q_x}{\partial x} + \frac{\partial Q_y}{\partial y} + n_x\frac{\partial^2 w}{\partial x^2} + \frac{aD(1 + \cos 2\beta)}{3\left(\frac{\alpha_{bt}}{6} + \alpha_{bb}\right)(3 + v)(1 - v)h + 2a}
$$
$$
\left(\frac{\partial^3 \phi_y}{\partial y^3} + v\frac{\partial^3 \phi_x}{\partial x^2 \partial y}\right) - \frac{a(1 + \cos 2\beta)}{(6\alpha_{tb} + \alpha_{tt})(1 - v^2)h + 2a}n_y\frac{\partial^2 w}{\partial y^2}
$$

$$+\frac{2a\sin 2\beta}{3\left(\frac{C_{bt}}{6}+C_{bb}\right)(1+v)h+2a}\left(\frac{\partial^4\phi_y}{\partial x\partial y^2}+v\frac{\partial^4\phi_x}{\partial x^2\partial y}\right) \tag{48}$$

$$-\frac{2a\sin 2\beta}{(6C_{tb}+C_{bttb})(1+v)h+2a}n_y\frac{\partial^2 w}{\partial x\partial y}+P_{blast}=I_0\frac{\partial^2 w}{\partial t^2},$$

$$\delta\phi_x: \quad \frac{\partial M_{xx}}{\partial x}+\frac{\partial M_{xy}}{\partial y}-Q_x=I_1\frac{\partial^2 u}{\partial t^2}+I_2\frac{\partial^2\phi_x}{\partial t^2}, \tag{49}$$

$$\delta\phi_y: \quad \frac{\partial M_{xy}}{\partial x}+\frac{\partial M_{yy}}{\partial y}-Q_y=I_1\frac{\partial^2 v}{\partial t^2}+I_2\frac{\partial^2\phi_\theta}{\partial t^2}, \tag{50}$$

where the stress resultant are

$$N_{xx}=A_{11}\frac{\partial u}{\partial x}+B_{11}\frac{\partial\phi_x}{\partial x}+A_{12}\frac{\partial v}{\partial y}+B_{12}\frac{\partial\phi_y}{\partial y}, \tag{51}$$

$$N_{yy}=A_{12}\frac{\partial u}{\partial x}+B_{12}\frac{\partial\phi_x}{\partial x}+A_{22}\frac{\partial v}{\partial y}+B_{22}\frac{\partial\phi_y}{\partial y}, \tag{52}$$

$$N_{xy}=A_{66}\left(\frac{\partial u}{\partial y}+\frac{\partial v}{\partial x}\right)+B_{66}\left(\frac{\partial\phi_x}{\partial y}+\frac{\partial\phi_y}{\partial x}\right), \tag{53}$$

$$Q_x=A_{55}\left(\frac{\partial w}{\partial x}+\phi_x\right), \tag{54}$$

$$Q_y=A_{44}\left(\frac{\partial w}{\partial y}+\phi_\theta\right), \tag{55}$$

$$M_{xx}=B_{11}\frac{\partial u}{\partial x}+D_{11}\frac{\partial\phi_x}{\partial x}+B_{12}\frac{\partial v}{\partial y}+D_{12}\frac{\partial\phi_y}{\partial y}, \tag{56}$$

$$M_{yy}=B_{12}\frac{\partial u}{\partial x}+D_{12}\frac{\partial\phi_x}{\partial x}+B_{22}\frac{\partial v}{\partial y}+D_{22}\frac{\partial\phi_y}{\partial y}, \tag{57}$$

$$M_{x\theta}=B_{66}\left(\frac{\partial u}{\partial y}+\frac{\partial v}{\partial x}\right)+D_{66}\left(\frac{\partial\phi_x}{\partial y}+\frac{\partial\phi_y}{\partial x}\right), \tag{58}$$

Finally, substituting above relations in motion equation results in final equations.

2.4 Solution

Considering the simply supported boundary condition, we have (Narendar and Gopalakrishnan 2012)

$$u(x,y,t)=u0(t)\cos\left(\frac{m\pi x}{a}\right)\cos\left(\frac{n\pi y}{b}\right), \tag{59}$$

$$v(x,y,t)=v0(t)\sin\left(\frac{m\pi x}{a}\right)\cos\left(\frac{n\pi y}{b}\right), \tag{60}$$

$$w(x,y,t)=w0(t)\sin\left(\frac{m\pi x}{a}\right)\sin\left(\frac{n\pi y}{b}\right), \tag{61}$$

$$\phi_x(x,y,t)=\phi_x0(t)\cos\left(\frac{m\pi x}{a}\right)\cos\left(\frac{n\pi y}{b}\right), \tag{62}$$

$$\phi_y(x,y,t)=\phi_y0(t)\sin\left(\frac{m\pi x}{a}\right)\cos\left(\frac{n\pi y}{b}\right), \tag{63}$$

where *a* and *b* are the length and width of plate, respectively; *m* and *n* are mode numbers in *x*- and *y*-

directions, respectively. Substituting Eqs. (59)-(63) into Eqs. (46)-(50) and using Galerkin method, we have

$$M\ddot{d}(t)+Kd(t)=Q(t), \tag{64}$$

where *M* and *K* are the mass and stiffness of the structure, respectively and d is the dynamic vector (i.e., $d=\{u_0, v_0, w_0, \phi_{x0}, \phi_{y0}\}$). In this section, Newmark method is applied in the time domain to obtain the time response of the structure under the blast load. Based on this method, Eq. (64) can be written in the general form as below (Simsek 2010)

$$K^*(d_{i+1})=Q_{i+1}, \tag{65}$$

where subscript *i*+1 indicates the time $t=t_{i+1}$, $K^*(d_{i+1})$ and Q_{i+1} are the effective stiffness matrix and the effective load vector which can be considered as

$$K^*(d_{i+1})=K+\alpha_0 M, \tag{66}$$

$$Q_{i+1}^*=Q_{i+1}+M\left(\alpha_0 d_i+\alpha_2\dot{d}_i+\alpha_3\ddot{d}_i\right), \tag{67}$$

where (Simsek 2010)

$$\alpha_0=\frac{1}{\chi\Delta t^2}, \qquad \alpha_1=\frac{\gamma}{\chi\Delta t}, \qquad \alpha_2=\frac{1}{\chi\Delta t},$$
$$\alpha_3=\frac{1}{2\chi}-1, \quad \alpha_6=\Delta t(1-\gamma), \qquad \alpha_7=\Delta t\gamma, \tag{68}$$

in which $\gamma=0.5$ and $\chi=0.25$. Based on the iteration method, Eq. (65) is solved at any time step and modified velocity and acceleration vectors are calculated as follows

$$\ddot{d}_{i+1}=\alpha_0(d_{i+1}-d_i)-\alpha_2\dot{d}_i-\alpha_3\ddot{d}_i, \tag{69}$$

$$\dot{d}_{i+1}=\dot{d}_i+\alpha_6\ddot{d}_i+\alpha_7\ddot{d}_{i+1}, \tag{70}$$

Then for the next time step, the modified velocity and acceleration vectors in Eqs. (69) and (70) are employed and all these procedures mentioned above are repeated.

3. Experimental test

As shown in Fig. 2, a concrete block with a close angled discontinues is considered where the geometrical parameters of it is length of 2 m, width of 1 m and thickness of 50 cm. A closed angle discontinues is located in this sample and two Geophones are considered before and after

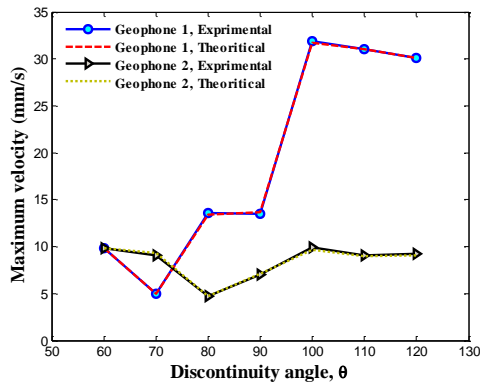Fig. 2 A concrete block with a close angled discontinues

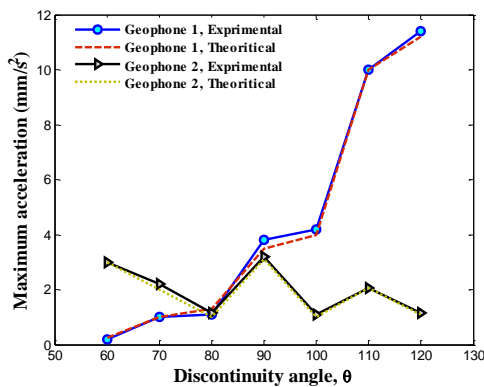Fig. 3 The maximum velocity of the concrete block for different angle of discontinues

Fig. 5 Velocity response of the concrete block for Geophone 1

Fig. 4 The acceleration of the concrete block for different angle of discontinues

Fig. 6 Velocity response of the concrete block for Geophone 2

of discontinues namely as Geophones 1 and 2, respectively. The blast hole with the diameter of 20 mm and height of 30 cm is built at the distance of 75 cm to Geophone 1 where the explosive material is Barit. The main objective of these tests is obtaining the maximum phase velocity at different discontinues angles and times which are discussed in the next section (Pourghasemi Sagand 2015).

4. Numerical results and discussion

In this section, the experimental and theoretical results are presented for a concrete block with a close angled discontinues. The elastic modules and Poisson's ratio of concrete are E_m=20 GPa and v_m=0.3, respectively. The concrete block is mixed with and SiO_2 nanoparticles with elastic modules of E_r=75 GPa and Poisson's ratio of v_r=0.27.

4.1 Experimental results

The velocity and acceleration of the concrete block related to Geophone 1 and 2 for different angle of discontinues are presented in Figs. 3 and 4, respectively. In these figures, the theoretical and experimental results are compared. As can be seen, the mathematical model presented in this paper has high accuracy since the velocity and acceleration obtained by Newmark method are math
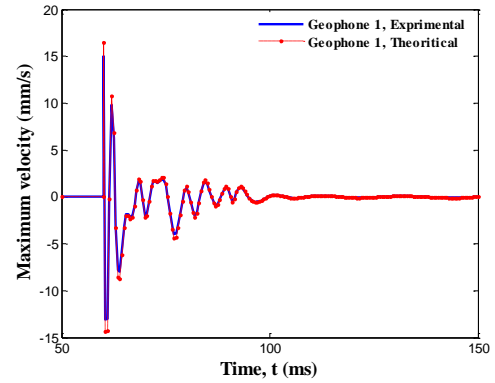
with experimental results, indication validation of this work. It is also concluded that the maximum velocity recorded by Geophone 1 (before discontinues) is higher than Geophone 2 (after discontinues) for angle of discontinues higher than 80°.

In another attempt for validation of the presented mathematical model, the velocity response of the structure is plotted in Figs. 5 and 6, respectively for Geophones 1 and 2. It can be observed that the velocity recorded by Geophone 1 (before discontinues) is higher than Geophone 2 (after discontinues). Furthermore, the theoretical results are close to the experimental datas. However, it can be concluded that the present model and formulation can predicts the exact results for the considered concrete structure.

4.2 Theoretical results

In this section, the effect of different parameters such as SiO_2 nanoparticles volume percent and agglomeration, angle of discounts, length, width and thickness of the concrete block are shown on the velocity response of the model.

Figs. 7 and 8 show the effect of SiO_2 nanoparticles volume percent and SiO_2 agglomeration on the velocity response of the concrete structure. As can be seen, with increasing the volume percent of SiO_2 nanoparticles, the maximum velocity of the structure is decreased. For
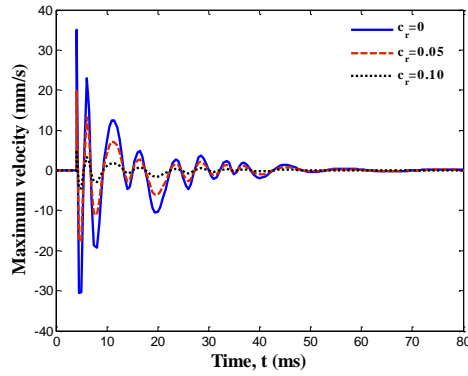
Fig. 7 The effect of SiO$_2$ nanoparticles volume percent on the velocity response of the concrete block
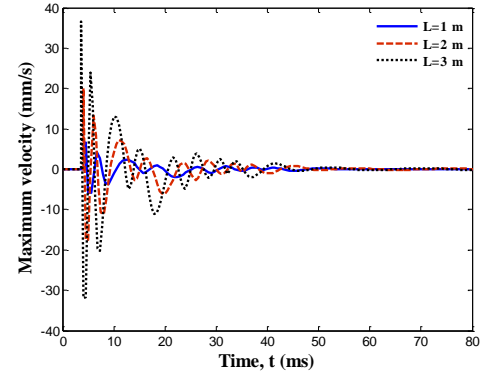

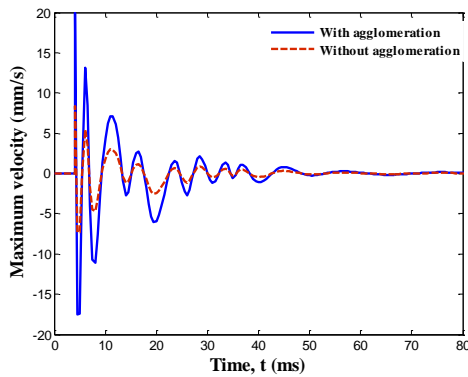Fig. 10 The effect of concrete block length on the velocity response of the concrete block

Fig. 8 The effect of SiO$_2$ agglomeration on the velocity response of the concrete block
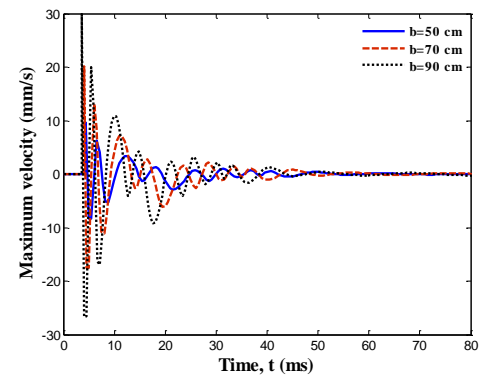

Fig. 11 The effect of concrete block width on the velocity response of the concrete block
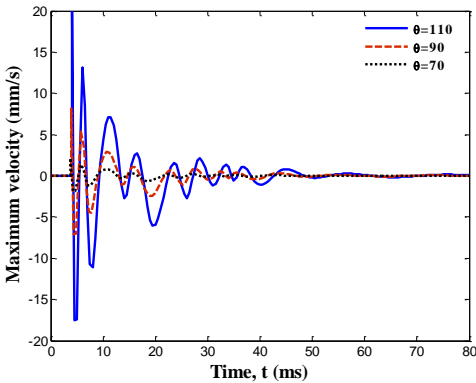

Fig. 9 The effect of discontinues angle on the velocity response of the concrete block
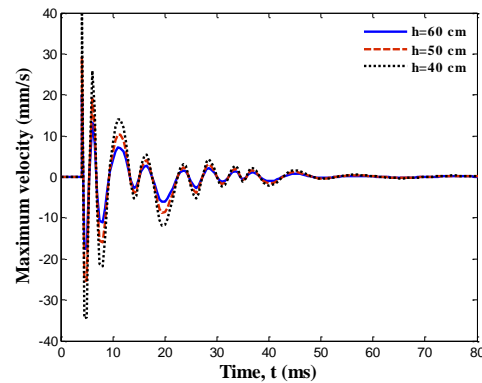

Fig. 12 The effect of concrete block thickness on the velocity response of the concrete block

example, using 0.05% SiO$_2$ nanoparticles, maximum velocity is reduced about 74%. It is physical due to this fact that with increasing the volume percent of SiO$_2$ nanoparticles, the rigidity and stiffness of the structure is improved. In addition, considering the agglomeration of SiO$_2$ nanoparticles leads to increase in the maximum velocity of the concrete block since the stability and homogeneity of system decreases.

Fig. 9 illustrates the effects of discontinues angle on the maximum phase velocity of the structure. It is shown that the maximum phase velocity increases with increasing discontinues angle. Noted that this result is the same as those reported in Fig. 3 for experimental tests.

Figs. 10-12, respectively demonstrate the effects of the length, width and thickness of the concrete block on the maximum velocity response of the structure. As can be seen, increasing the length and width as well as decreasing the thickness of the structure causes to increase in the maximum velocity of the concrete structure. It is due to the fact that increasing the length and width as well as decreasing the thickness of the structure leads to lower stiffness in the structure.

5. Conclusions

For the first time, a mathematical model was presented in this paper for predicting the blast response of the concrete block. The structure was reinforced SiO_2 nanoparticles considering the agglomeration effects. Applying CPT, energy method and Hamilton's principle, the motion equation was derived. Based on exact solution and Newmark method, the maximum velocity of the structure was obtained and compared with the experimental tests. The effect of different parameters such as SiO_2 nanoparticles volume percent and agglomeration, angle of discontinues, length, width and thickness of the model were shown on the maximum velocity of the model. Results indicate that the theoretical results were in a good agreement with the experimental datas. The most finding of this paper are:

√ The maximum velocity of the before discontinues was higher than after of discontinues.

√ With increasing the volume percent of SiO_2 nanoparticles up to 0.05%, the maximum velocity decreases 74 percent.

√ Considering SiO_2 nanoparticles agglomeration leads to increase in the maximum velocity of the structure.

√ Increasing the length and width as well as decreasing the thickness of the structure causes to increase in the maximum velocity of the concrete structure.

Finally, it is hoped that this work open a new field in the mining engineering for mathematical modelling of the structure in order to predict the blast response of them.

References

Aliabadian, Z., Sharafisafa, M., Mortazavi, A. and Maarefvand, P. (2014), "Wave and fracture propagation in continuum and faulted rock masses: distinct element modeling", *Arab. J. Geosci.*, **7**, 5021-5035.

Bayraktar, A., Türker, T., Altunişik, A.C. and Sevim, B. (2010), "Evaluation of blast effects on reinforced concrete buildings considering Operational Modal Analysis results", *Soil Dyn. Earthq. Eng.*, **30**, 310-319.

Brush, O. and Almorth, B. (1975), *Buckling of Bars, Plates and Shells*, Mc-Graw Hill.

Dadsetan, S. and Bai, J. (2017), "Mechanical and microstructural properties of self-compacting concrete blended with metakaolin, ground granulated blast-furnace slag and fly ash", *Constr. Build. Mater.*, **146**, 658-667.

Hause, T. and Librescu, L. (2007), "Dynamic response of doubly-curved anisotropic sandwich panels impacted by blast loadings", *Int. J. Solid. Struct.*, **44**, 6678-6700.

Ismail, R. and Cartmell, M.P. (2012), "An analysis of the effects of the orientation angle of a surface crackon the vibration of an isotropic plate", *J. Phys.: Conf. Ser.*, **382**, 012007.

Jayasooriy, R., Thambiratnam, D.P., Perera, N.J. and Kosse, V. (2011), "Blast and residual capacity analysis of reinforced concrete framed buildings", *Eng. Struct.*, **33**, 3483-3495.

Jeon, S., Kim, T.H. and You, K.H. (2015), "Characteristics of crater formation due to explosives blasting in rock mass", *Geomech. Eng.*, **9**, 329-344.

Joseph, P.F. and Erdogan, F. (1991), "Surface crack in a plate under antisymmetric loading conditions", *Int. J. Solid. Struct.*, **27**, 725-750.

Kim, H.J., Yi, N.H., Kim, S.B., Nam, J.W., Ha, J.H. and Kim Jay, J.H. (2011), "Debonding failure analysis of FRP-retrofitted concrete panel under blast loading", *Struct. Eng. Mech.*, **38**, 479-501.

Kinney, G.F. and Graham, KJ. (1985), *Explosive Shock*, Springer-verlag, Newyork.

Kyei, C. and Braimah, A. (2017), "Effects of transverse reinforcement spacing on the response of reinforced concrete columns subjected to blast loading", *Eng. Struct.*, **142**, 148-164.

Li, G.Q., Yang, T.Ch. and Chen, S.W. (2009), "Behavior and simplified analysis of steel-concrete composite beams subjected to localized blast loading", *Struct. Eng. Mech.*, **32**, 337-350.

Li, J., Ma, G. and Huang, X. (2010), "Analysis of wave propagation through a filled rock joint", *Rock Mech, Rock Eng.*, **43**, 789-798.

Li, X., Wang, E., Li, Zh., Bie, X., Chen, L., Feng, J. and Li, N. (2016), "Blasting wave pattern recognition based on Hilbert-Huang transform", *Geomech. Eng.*, **11**, 607-624.

Lu, Y.C. and Xu, Y.G. (1986), "Line-spring model for a surface crack loaded antisymmetrically", National University of Defense Technology Technical Paper.

Luccioni, B., Isla, F., Codina, R., Ambrosini, D., Zerbino, R., Giaccio, G. and Torrijo, M.C. (2017), "Effect of steel fibers on static and blast response of high strength concrete", *Int. J. Impact Eng.*, **107**, 23-37.

Ma, H.M., Gao, X. L. and Reddy, J.N. (2011), "A non-classical Mindlin plate model based on a modified couple stress theory", *Acta Mech.*, **220**, 217-235.

Mori, T. and Tanaka, K. (1973), "Average stress in matrix and average elastic energy of materials with misfitting inclusions", *Acta Metall. Mater.*, **21**, 571- 574.

Nam, J.W., Kim, H.J., Yi, N.H., Kim, I.S., Jay Kim, J.H. and Choi, H.J. (2009), "Blast analysis of concrete arch structures for FRP retrofitting design", *Comput. Concrete*, **6**, 305-318.

Oña, M., Morales-Alonso, G., Gálvez, F., Sánchez-Gálvez, V. and Cendón, D. (2016), "Analysis of concrete targets with different kinds of reinforcements subjected to blast loading", *The Europ. Phys. J. Spec. Top.*, **225**, 265-282.

Petel, O.E., Jetté, F.X., Goroshin, S., Frostm D.L. and Ouellet, S. (2011), "Blast wave attenuation through a composite of varying layer distribution", *Shock Wav.*, **21**, 215-224.

Pourghasemi Sagand, M. (2015), "The experimental study of the effects of discontinously on the Blast-induced energy partitioning in resistant rocks", MSc Theses, University of Tehran.

Rice, J.R. and Levy, N. (1972), "The part-through surface crack in an elastic plate", *J. Appl. Mech.*, **39**, 185-194.

Shi, D.L. and Feng, X.Q. (2004), "The effect of nanotube waviness and agglomeration on the elastic property of carbon nanotube reinforced composties", *J. Eng. Mat. Tech.*, ASME, **126**, 250-270.

Simsek, M. (2010), "Non-linear vibration analysis of a functionally graded Timoshenko beam under action of a moving harmonic load", *Compos. Struct.*, **92**, 2532-2546.

Wu, Y.K., Hao, H., Zhou, Y.X. and Chong, K. (1998), "Propagation characteristics of blast-induced shock waves in a jointed rock mass", *Soil Dyn. Earthq. Eng.*, **17**, 407-412.

Yoo, D.Y. and Banthia, N. (2017), "Mechanical and structural behaviors of ultra-high-performance fiber-reinforced concrete subjected to impact and blast", *Constrt. Build. Mater.*, **149**, 416-431.

CC